The Canadian Mineralogist
Vol. 45, pp. 945-962 (2007)
DOI: 10.2113/gscanmin.45.4.945

DISSOLUTION OF URANYL-OXIDE-HYDROXY-HYDRATE MINERALS. III. BILLIETITE

MICHAEL SCHINDLER[§], FRANK C. HAWTHORNE AND NORMAN M. HALDEN

Department of Geological Sciences, University of Manitoba, Winnipeg, Manitoba R3T 2N2, Canada

PETER C. BURNS AND PATRICIA A. MAURICE

Department of Civil Engineering and Geological Sciences, University of Notre Dame, Notre Dame, Indiana 46556-0767, USA

ABSTRACT

Dissolution experiments on freshly cleaved and non-freshly cleaved single crystals of billietite, $Ba(H_2O)_8[(UO_2)_6O_4(OH)_6]$, were done in HCl solutions of pH 2, in ultrapure water, in 0.1 mol L^{-1} Na_2CO_3 solutions of pH 10.5, in 1.0 mol L^{-1} *M*Cl solutions of pH 2 (*M* = Na, K, Li), in 0.5 mol L^{-1} MCl_2 solutions of pH 2 (*M* = Ca, Sr, Mg) and in a 0.5 mol L^{-1} $Pb(NO_3)_2$ solution of pH 2. Dissolution features on the (001) basal surface of the billietite crystals were examined with atomic-force microscopy, scanning electron microscopy and optical microscopy. Hillocks on the basal surface form in ultrapure water, and a striped pattern of steps occurs on the billietite surface after treatment in a Na_2CO_3 solution of pH 10.5. Etch pits form only on the basal surface in solutions of pH 2, indicating that their formation is promoted by a higher activity of protons in solution. Symmetry and elongation of etch pits formed in electrolyte solutions of pH 2 can vary with the type of surface (*i.e.*, freshly cleaved *versus* non-freshly cleaved) and the cation in solution. Etch pits on non-freshly cleaved surfaces commonly display a lower symmetry than the etch pits formed on freshly cleaved surfaces, most likely the result of the degree of alteration of the non-freshly cleaved surfaces. Etch pits elongate parallel to [100] form in aqueous NaCl, KCl and $MgCl_2$ solutions, and etch pits elongate parallel to [010] form in aqueous $CaCl_2$, $SrCl_2$ and $Pb(NO_3)_2$ solutions, respectively. A Pb^{2+}-containing phase precipitates on the surface in an aqueous $Pb(NO_3)_2$ solution of pH 2. Etch pits formed on billietite in Ca-containing solutions are elongate parallel to the rows of Ca atoms in the bulk structure of becquerelite, $Ca(H_2O)_8[(UO_2)_6O_4(OH)_6]$, and to the elongation of the becquerelite crystals. The different elongation of etch pits can be explained with an adsorption model involving the cations in solution and specific sites on the basal surface. In the electrolyte solutions, the relief of dissolution features on the basal surface and edges increases in the sequence KCl < $Pb(NO_3)_2$ < $SrCl_2$ < NaCl < $CaCl_2$ = $MgCl_2$ = LiCl, suggesting that the relief of the basal surface inversely correlates with the size of the cation in solution.

Keywords: billietite, dissolution, etch pit, surface, uranyl oxide minerals, bond valence.

SOMMAIRE

Nous avons étudié la dissolution globale de monocristaux de billietite, $Ba(H_2O)_8[(UO_2)_6O_4(OH)_6]$, fraichement clivés ou non, dans des solutions de HCl de pH 2, dans l'eau ultrapure, dans une solution de Na_2CO_3, 0.1 mol L^{-1} d'un pH de 10.5, une solution de *M*Cl (*M* = Na, K, Li), 1.0 mol L^{-1}, d'un pH de 2, une solution de MCl_2 (*M* = Ca, Sr, Mg), 0.5 mol L^{-1}, d'un pH de 2, et une solution de $Pb(NO_3)_2$, 0.5 mol L^{-1}, d'un pH de 2. Les manifestations de la dissolution sur la face (001) des cristaux de billietite ont été examinées par microscopie à force atomique, microscopie électronique à balayage, et microscopie optique. Des amoncellements sur la surface (001) se développent dans l'eau ultrapure, et un agencement rubanné d'échelons se développe sur la surface de la billietite après traitement dans une solution de Na_2CO_3 d'un pH de 10.5. Les figures de corrosion se développent seulement sur la surface de base dans des solutions de pH 2, indication que leur formation est promue par une activité accrue de protons en solution. La symétrie et l'allongement des figures de corrosion formées dans des solutions d'électrolytes de pH 2 peuvent varier selon la surface, fraichement clivée ou non, et la nature du cation en solution. Les figures de corrosion sur les surfaces non fraichement clivées montrent en général une symétrie plus basse que celles qui sont développées sur les surfaces fraichement clivées, résultat probable du degré d'altération des surfaces vieillies. Les figures de corrosion allongées parallèles à [100] se forment dans des solutions aqueuses de NaCl, KCl et $MgCl_2$, et celles qui sont allongées parallèles à [010] se forment dans des solutions aqueuses de $CaCl_2$, $SrCl_2$ and $Pb(NO_3)_2$, respectivement. Un composé de Pb^{2+} a précipité sur la surface dans une solution aqueuse de $Pb(NO_3)_2$ de pH 2. Les figures de corrosion formées sur la billietite dans des solutions contenant le Ca sont allongées parallèles aux rangées d'atomes Ca dans la structure de la becquerelite, $Ca(H_2O)_8[(UO_2)_6O_4(OH)_6]$, et à l'allongement

§ Present address: Department of Earth Sciences, Laurentian University, Sudbury, Ontario P3E 2C6, Canada. *E-mail address*: mschindler@laurentian.ca

des cristaux de becquerelite. Les différences notées dans l'allongement des figures de corrosion auraient une explication dans l'absorption impliquant les cations en solution et les sites spécifiques sur la surface (001). Dans les solutions d'électrolytes, le relief des figures de dissolution sur cette surface et le long des arêtes augmente selon la séquence KCl < $Pb(NO_3)_2$ < $SrCl_2$ < NaCl < $CaCl_2$ = $MgCl_2$ = LiCl, ce qui laisse supposer une corrélation inverse entre le relief et la taille du cation en solution.

(Traduit par la Rédaction)

Mots-clés: billietite, dissolution, figure de corrosion, surface, minéraux oxydes à uranyle, valence de liaison.

Introduction

Uranyl-oxide-hydroxy-hydrate minerals are common constituents of the oxidized parts of uranium deposits (Frondel 1958, Finch & Ewing 1992) and soils contaminated by actinides (Roh *et al*. 2000, Yamakawa & Traina 2001). They are prominent alteration-induced phases in laboratory experiments involving UO_2 and spent nuclear fuel in a moist, oxidizing environment similar to the proposed repository at Yucca Mountain (Wronkiewicz *et al.* 1996, Finn *et al.* 1996, Finch *et al.* 1999). Short-term dissolution experiments on uranyl-oxide-hydroxy-hydrate minerals can be used to assess models for the prediction of long-term behavior of spent nuclear fuel in a geological repository. Here, we examine the dissolution of the uranyl-hydroxy-hydrate mineral billietite as a function of pH and the type of cation in solution.

Billietite, $Ba(H_2O)_8[(UO_2)_6O_4(OH)_6]$, contains Ba, one isotope of which is a fission product in spent nuclear fuel. A phase with a structure similar to that of billietite, but which contains Cs, Ba, and Mo in addition to U, was reported from experiments on the oxidative corrosion of spent nuclear fuel in groundwater (Buck *et al.* 1998). Many of the radionuclides released from spent nuclear fuel during alteration in a geological repository may be either incorporated into uranyl-oxide-hydroxy-hydrates (Burns *et al.* 1997, 2004, Burns & Li 2002, Chen *et al.* 1999, 2000, Douglas *et al.* 2005) or adsorbed on their surface (Schindler *et al.* 2006a, b, 2007). The adsorption of radionuclides on the surface of minerals can be examined *via* simple dissolution-type experiments, because adsorption and dissolution are surface processes that can interfere with each other. Adsorption of cations at specific surface-sites can modify the orientation, morphology and relief of dissolution features, which can provide insight into the fate of alteration products of spent nuclear fuel in a geological repository.

Previous Experiments on the Dissolution of Uranyl-Hydroxy-Hydrate Minerals

Numerous bulk-dissolution experiments on uranyl minerals and synthetic uranyl phases have been done (*e.g.*, Vochten *et al.* 1991, 1995, Sandino & Bruno 1992, Sandino & Grambow 1994, Torrero *et al.* 1994, Casas *et al.* 1997). Bulk-disolution experiments on becquerelite and schoepite show that the lowest solubilities of these minerals occur in the pH range 7–8 (Torrero *et al.* 1994, Casas *et al.* 1997). The influence of dissolved Na and Cs aqueous species on the dissolution of metaschoepite was examined in bulk-dissolution experiments at pH 6 by Giammar & Hering (2004). Here, the authors reported complex dissolution-reprecipitation processes in all experiments and, as a result, the formation of Na- and Cs-bearing uranyl-hydroxy-hydrate phases. Solubility data from bulk-dissolution experiments on billietite have not been yet reported.

Two recent studies on dissolution of the basal surfaces of curite, $Pb^{2+}{}_3(H_2O)_2[(UO_2)_4O_4(OH)_3]_2$, and becquerelite, $Ca(H_2O)_8[(UO_2)_6O_4(OH)_6]$, showed that the formation of etch pits is favored by an increasing degree of protonation of edges, whereas the formation of hillocks is favored by a decreasing degree of protonation (Schindler *et al.* 2006a, b). The dissolution experiments on the basal surface of curite also revealed that with increasing degree of protonation of edges, etch pits grow faster laterally than perpendicular to the basal surface. Schindler *et al.* (2006a, b) observed that the general symmetry of the etch pits formed in HCl and H_2O solutions does not reflect the symmetry of the bulk structure, which they explained with different rates of dissolution perpendicular to edges of left and right terminations and with a nonstoichiometric process of dissolution.

Dissolution experiments with different electrolyte solutions of pH 2 on the basal surface of becquerelite showed that the elongation of etch pits changes with the type of cation in solution. Schindler *et al.* (2006b) explained this phenomenon with an adsorption model developed on the basis of a protonation model of the equatorial anion-terminations on the basal face and its edges. Here, the cations in solution bond to the O atoms of the uranyl groups on the basal face rather than to the equatorial atoms of oxygen of the uranyl polyhedra. The cations adsorbed on the basal face prevent (1) attachment of a hydronium ion and subsequent protonation of the equatorial atoms of oxygen in its immediate surroundings, and (2) detachment of a cluster or a polyhedron perpendicular to the row of cations. The experiments also showed that the lateral dimensions of etch pits, the shape of edges along etch pits, and the relief of dissolution features on edges of the basal surface vary with the type of cation in solution. Schindler *et al.* (2006b) explained the variation in the relief of the dissolution features by invoking the role of the cations in solution during a surface-controlled disso-

lution process (Stumm 1992): (1) dissolution inhibitors: cations of the solution are adsorbed on the surface and inhibit protonation of the equatorial atoms of oxygen; (2) dissolution promoters: cations of the solution form complexes with detached polyhedra or groups of polyhedra by bonding to their O atoms.

The results of the dissolution experiments on curite and becquerelite can be summarized as follows: [1] In solutions without alkaline and earth-alkaline cations, the dissolution process is controlled by nonstoichiometric detachment of components of the interstitial complex and the sheet of polymerized uranyl-polyhedra (structural unit). [2] In the presence of alkaline and earth-alkaline cations in solution, the dissolution process is strongly controlled by the adsorption of the corresponding cation on the basal surface of the uranyl-hydroxy-hydrate mineral.

Objectives of this paper

The structure of billietite, $Ba(H_2O)_8[(UO_2)_6O_4(OH)_6]$, contains a sheet of uranyl polyhedra that has the same anion topology and chemical composition as the sheet of uranyl polyhedra in becquerelite. The major difference between the structures of billietite and becquerelite is the chemical composition and arrangement of the interstitial complex. Billietite is not a common mineral in the vadose zone of uranium deposits. However, dissolution studies on its basal surface can provide answers to the following questions regarding the dissolution of uranyl-oxide-hydroxy-hydrate minerals:

(1) How does the chemical composition and arrangement of the interstitial complex in billietite affect (a) the nonstoichiometric dissolution process? (b) the occurrence of etch pits and hillocks? (c) the morphology, orientation and relief of dissolution features?

(2) Do minerals with the same structural unit (becquerelite and billietite) have an identical structure on their basal surface? If they do, does the same cation in solution adsorb to the same surface-site, and does a similar adsorption result in a similar stability of the edges on and along the basal surface?

(3) Furthermore, we can combine questions (1) and (2): do the adsorbed cations on the surface or the interstitial complexes in the vicinity of the surface have a larger impact on the relief, orientation, and morphology of dissolution features?

(4) The surfaces of non-freshly cleaved uranyl minerals are altered through their interaction with solutions and the atmosphere. Hence, the structure and composition of this type of surface differ from those of freshly cleaved crystals. Differences in the structure and composition of surfaces result in different interactions with solutions, *i.e.* protonation of anion terminations and etch-pit nucleation. In this way, we want to investigate the differences in orientation and morphology of etch pits formed on the surfaces of freshly and non-freshly cleaved crystals of billietite.

Billietite and Becquerelite: Structural Unit, Interstitial Cations and Crystal Morphologies

The crystal structure of billietite, $Ba[(UO_2)_6O_4(OH)_6](H_2O)_8$, has an orthorhombic symmetry, space group $Pbn2_1$, with a 12.0941(8), b 30.211(2), c 7.563(5) Å (Finch *et al.* 2006). The structure consists of anionic $[(UO_2)_6O_4(OH)_6]^{2-}$ sheets, linked by interstitial Ba and (H_2O) groups. Figure 1a shows parts of the structural unit in which the pentagonal–bipyramidal uranyl polyhedra share common edges and corners through equatorial O^{2-} and $(OH)^-$ groups. The (OH) groups occur at some of the corners of the triangular holes in the sheet of polyhedra. The structural unit of billietite is identical to the structural units in becquerelite, $Ca(H_2O)_8[(UO_2)_6O_4(OH)_6]$ (Burns & Li 2002, Pagoaga *et al.* 1987), and compreignacite, $K_2(H_2O)_3[(UO_2)_6O_4(OH)_6]$ (Burns 1998, 1999). We will use the orientation *cab* and the dimensions a 7.563(5) b 12.0941(8), c 30.211 / 2 = 15.055 Å to describe the morphology and the orientation of chains of polyhedra in the structural unit, which is identical to the orientation used in our previous papers (Schindler *et al.* 2004a, b, 2006b). The space group of the billietite structure in this orientation is $P2_1cn$ (plane group 2*mm*).

Figures 1b, c show the arrangements of the interstitial cations Ca and Ba in becquerelite, and billietite, respectively. The interstitial Ca atoms in becquerelite are arranged in rows parallel to [010], whereas the interstitial Ba atoms in billietite (and compreignacite: Burns 1998) are arranged in rows parallel to [100].

Morphology, twinning and intergrowth of billietite crystals

Billietite and compreignacite crystals are commonly elongate parallel to [100], whereas becquerelite crystals are elongate parallel to [010] (Figs. 1b, c; Perloff 1998; http://www.trinityminerals.com/sm2001/uranium.shtml, Protas 1964). The basal surface is commonly bound by [110] and [100] edges in billietite and by [100], [110] and [010] edges in becquerelite. Twinning of billietite crystals is common on [111] and [110]; the latter twinning occurs commonly, and produces pseudohexagonal crystals (Schoep & Stradiot 1948). Figure 2 shows typical crystals of billietite used in the dissolution experiments described below. In both cases, the twinning occurs on [110]. The twinned crystals can be slightly elongate (Fig. 2a) or occur as pseudohexagonal tablets (Fig. 2c). The twinning of the crystals results in two different orientations of the etch pits on the basal surface of billietite (Figs. 2b, c). In some cases, parts of the billietite crystals can show an intergrowth of crystal

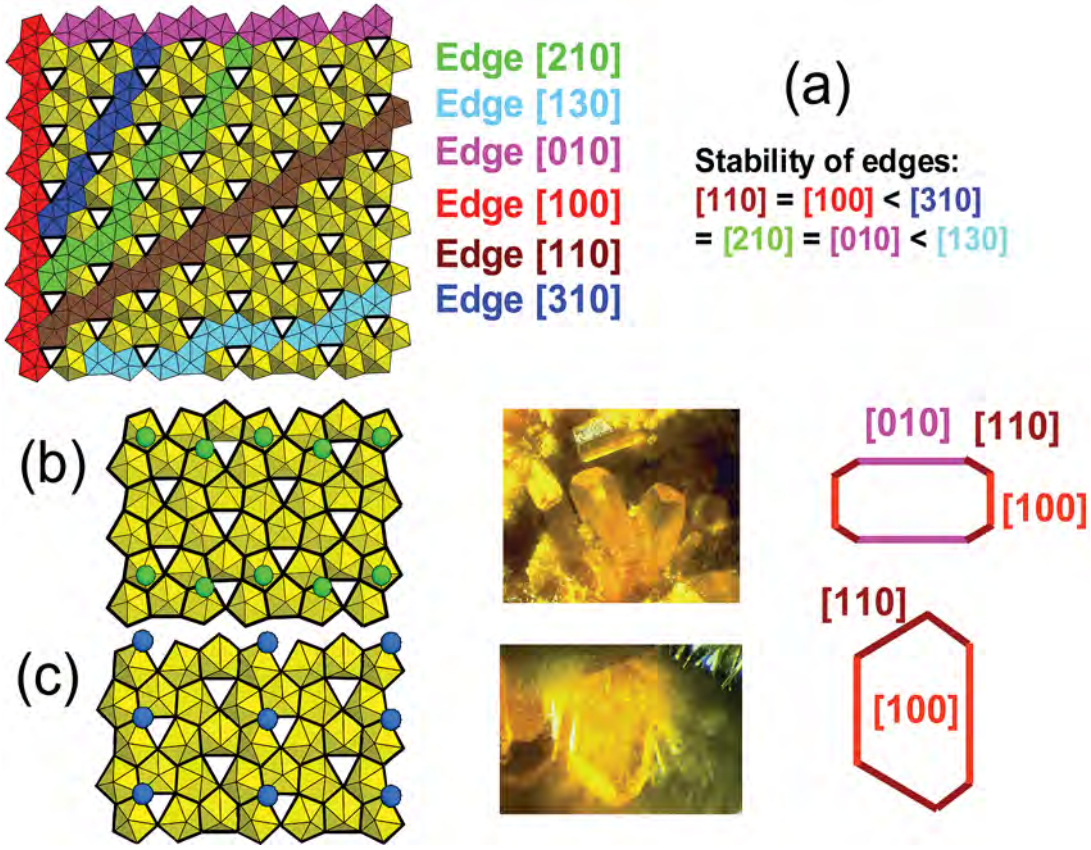

FIG. 1. (a) Polyhedron representation of the uranyl-oxide-hydroxy-hydrate sheet in billietite; polyhedron chains parallel to [100], [010], [110], [210], [310] and [130] are highlighted in red, pink, brown, green, dark blue and light blue, respectively, and the positions of the (OH) groups are shown as vertices of black triangles; (b), (c) polyhedron illustrations of layers in (b) becquerelite and (c) billietite, showing the positions of interstitial Ca (green circles) and Ba (blue circles); on the right: examples of the corresponding (001) surface morphologies on becquerelite and billietite crystals (for details, see text).

fragments with different orientations. As a result, etch pits on the surface of each fragment have a different orientation (Fig. 2b).

PREDICTION OF THE STABILITY OF EDGES ON THE BASAL SURFACE OF MINERALS WITH THE $[(UO_2)_6O_4(OH)_6]^{2-}$ STRUCTURAL UNIT

Schindler *et al.* (2004a) developed a new approach to calculate the stability of edges on basal surfaces of uranyl-sheet minerals. They determined the stability of an edge from (1) the bond-valence deficiency of chains of polyhedra parallel to those edges, (2) the arrangement of the interstitial complexes, and (3) the shift between the layers. This approach has been used to predict the morphology of basal surfaces of uranyl-sheet minerals (Schindler *et al.* 2004b) and to explain growth features of schoepite, $[(UO_2)_8O_2(OH)_{12}](H_2O)_{12}$ (Schindler & Putnis 2004), becquerelite, and wyartite, $Ca[U^{5+}(UO_2)_2(CO_3)O_4(OH)](H_2O)_7$ (Schindler *et al.* 2004c). Furthermore, Schindler *et al.* (2006a, b) applied this approach to the stability of edges of etch pits on the basal (100) surfaces of curite, $Pb^{2+}{}_3(H_2O)_2[(UO_2)_4O_4(OH)_3]_2$, and becquerelite.

Considering only the bond-valence deficiency and the shift between the layers (not the arrangement of the interstitial species), Schindler *et al.* (2004b, 2006b) predicted that in minerals with the becquerelite structure, the [110] and [100] edges are the most stable edges, followed by [010], [210] and [310] (Fig. 1a). This prediction is in agreement with observations on natural crystals, where the [110] and [100] edges always bound the basal surfaces (Figs. 1b, c, 2a, c). As described above, crystals of the becquerelite-group minerals

are elongate parallel to the arrangement of interstitial complexes. A possible explanation of this phenomenon is given in detail by Schindler *et al.* (2004a, 2006b).

Experimental

Billietite samples

The specimen containing billietite is from the William Pinch collection at the Canadian Museum of Nature and is from Shaba, Democratic Republic of Congo.

Dissolution experiments

We used two different sets of billietite crystals. One set contained crystals of different dimensions and was used to investigate the interaction between non-freshly cleaved surfaces and solutions of different pH and composition (named *set 1*). The second set contained crystals of similar dimension (named *set 2*) and was used to (a) investigate the interaction between freshly cleaved surfaces and solutions of different pH, and (b) compare the relief of the treated surfaces after the dissolution experiment.

For each dissolution experiment, we selected one platy crystal; the size of the basal surfaces of the crystals of the first set varied between 0.5 × 0.6 and 1.0 × 1.2 mm and of the second set, between 0.6 × 1.4 and 0.8 × 1.2 mm. Each crystal was placed in a small polyethylene cup that contained 10 mL of a solution of specific pH and composition. In Table 1, we list the types and concentrations of electrolyte solutions used, their pH and their ionic strengths; note that the electrolyte solutions of pH 2.0 have equal normality. All dissolution experiments were done at room temperature. The experiment in ultrapure water ran for 24 h (only for set 1), the experiments in solutions of pH 2 for 1½ h

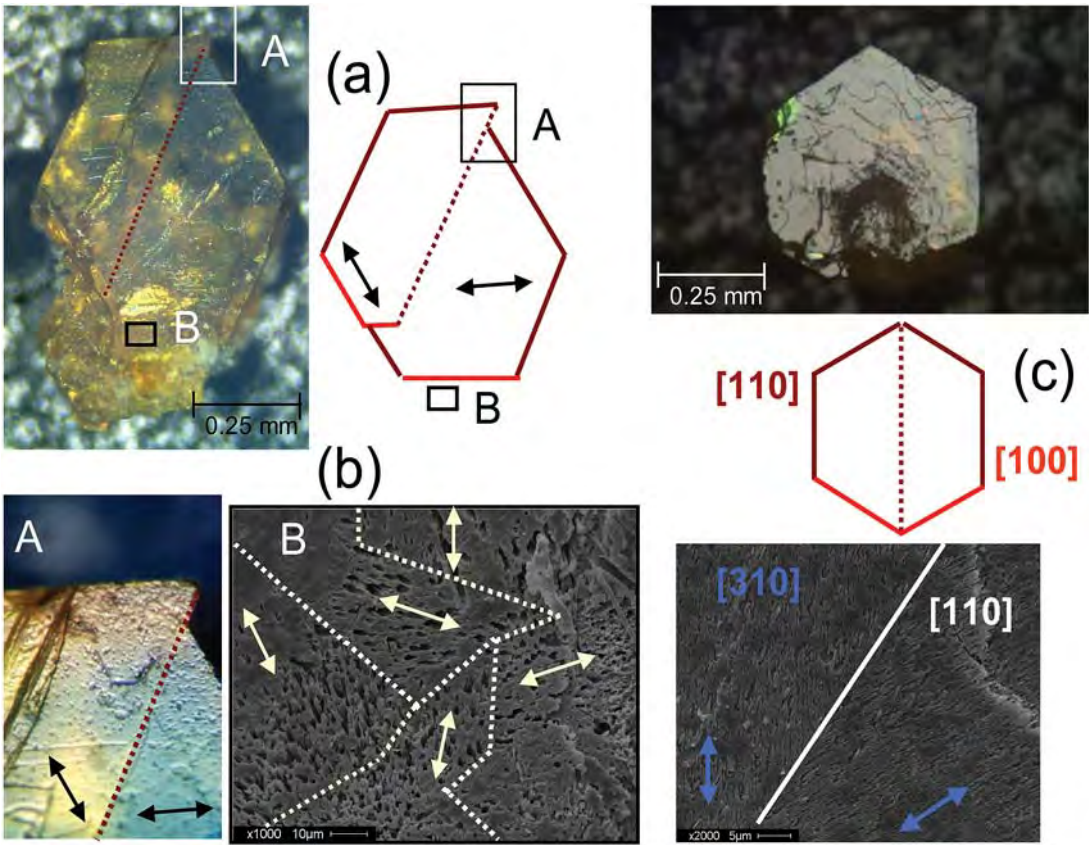

FIG. 2. (a) Optical-reflection microscopy image of a crystal of billietite showing twinning and intergrowth. (b) Optical-reflection microscopy and SEM images of the areas A and B in 2(a), indicating different orientation of etch pits due to twinning and intergrowth. (c) SEM images of a billietite crystal with a pseudohexagonal twinning (top) and orientation of etch pits close to the twin plane (bottom).

(set 1) and 2 h (set 2), and the experiment at pH 10.5 ran 1½ and 24 h (only for set 1). After the experiment, the crystals were quickly washed in pure water, dried in air (by touching their edge to a tissue) and mounted for atomic-force microscopy (AFM), optical-reflection microscopy and scanning electron microscopy (SEM). All AFM experiments were done shortly after the experiment (maximum one h). As for the dissolution experiments on curite and becquerelite, we did not do any *in situ* dissolution experiments (for details, see Schindler *et al.* 2006a, b). The ionic strengths of the electrolyte solutions were calculated using Visual MINTEQ 2.22 (Gustafsson 2003) and PHREEQC (Parkhurst 2003).

Atomic-force microscopy and scanning electron microscopy

After the dissolution experiments, the (001) surface of the billietite crystals was examined with a Digital Instruments Nanoscope III AFM with an extended module for phase imaging. The surface was scanned with a standard silicon nitride (Si_3N_4) contact-mode tip in air. In order to verify that scanning of the tip in contact mode over the surface did not induce erosion of the surface, altering the pit shape, or that drift did not substantially alter pit shape, we scanned an area twice in orthogonal directions. The AFM images were subsequently analyzed and modified with the *Flatten* and *Planefit* procedures, which correct the images for sample tilt, linear and oscillating drifts. Images in deflection and height mode were also modified with the zoom option of the AFM software. Note that the values for the depth of etch pits given in the figures and text sections are the measured values of how much the tip was able to penetrate the pit before contacting the opposite edge. The scanning electron microscopy studies were done with a 120 Stereoscan instrument from Cambridge Instruments; the crystals were analyzed with the Genesis 4000 EDAX system.

Laser-ablation – inductively coupled plasma – mass spectroscopy (*LA–ICP–MS*)

The billietite crystal that was treated with an aqueous $Pb(NO_3)_2$–HCl solution of pH 2 for 1½ h (set 1) was examined with LA–ICP–MS using a Merchantek LUV 134 laser coupled to a Thermo-Finnigan Element 2 inductively coupled plasma – mass spectrometer. The ablated material (coating and mineral) was monitored in time-resolved mode using single laser-shots. Laser-beam spot-sizes of 120–160 μm were used, depending on the size of the basal surface. The laser setting was at 30° with an incident pulse energy of 0.007 mJ and an energy density on the sample of 0.04 J/cm^2. The ablated material was semiquantitatively analyzed for the isotopes ^{206}Pb, ^{207}Pb and ^{208}Pb in depth-profile and line-scan modes to determine if a Pb-bearing phase was precipitated on the surface of billietite.

Fourier-transform infrared (*FTIR*) *spectroscopy*

The FTIR spectrum was recorded using a Bruker Hyperion 2000 infrared microscope equipped with a mercury cadmium telluride (MCT) detector. Spectral resolution was 4 cm^{-1} in the frequency range 4000 to 600 cm^{-1}. A billietite crystal treated with a Na_2CO_3 solution for 24 h (set 1) was mounted on a double-sided carbon tape, and the transmission spectrum was recorded in reflection mode.

Dissolution Features Observed on Billietite

Figures 3a and 3b show typical etch-pits on the basal (001) surface of billietite after treatment with an aqueous HCl solution of pH 2 for 1.5 h (set 1). The etch pits are elongate parallel to [100], and bound by the edges [100] and [110]; they merge to form larger pits that extend along [010]. Individual etch-pits can be identified by different colors, indicating different depths. The terminations on the [010] edge are irregular and characterized by small indentations; as a result, the outline of the etch pits displays plane-group symmetry 1.

The basal surface treated with solutions of higher pH

Figure 3c shows rounded hillocks on the basal (001) surface of billietite (set 1) after dissolution in ultrapure water. These rounded hillocks merge to form ripples that have a diameter of ~300 nm and a maximum height of ~20 nm (Fig. 3d). Figures 4a and 4b show the occurrence of a striped pattern of steps on the basal surface of billietite (set 1), which formed during dissolution in an aqueous Na_2CO_3 solution of pH 10.5. The steps are elongate parallel to [310], and each step is characterized by a flat surface and is bound by edges that are parallel to [110] and [100] of the billietite crystal. A cross section shows that the steps have diameter greater than 1.0 μm and a maximum height of ~60 nm (Fig. 4c). Careful inspection of the deflection image (Fig. 4a) and

TABLE 1. DISSOLUTION EXPERIMENTS ON BILLIETITE: CONCENTRATION OF ELECTROLYTE SOLUTION, pH AND IONIC STRENGTH

Electrolyte solution	pH value (measured)	Ionic strength (calculated)
0.5 mol L^{-1} $BaCl_2$ x nH_2O	2.0	1.23
0.5 mol L^{-1} $SrCl_2$ x nH_2O	2.0	1.15
0.5 mol L^{-1} $MgCl_2$ x nH_2O	2.0	0.98
0.5 mol L^{-1} $Pb(NO_3)_2$ x nH_2O	2.0	0.51
1.0 mol L^{-1} LiCl	2.0	0.84
1.0 mol L^{-1} NaCl	2.0	0.84
1.0 mol L^{-1} KCl	2.0	1.14
HCl	2.0	0.001
Ultrapure H_2O	7.0[1]	0
0.1 mol L^{-1} Na_2CO_3	10.5	0.2

[1] theoretical value.

the cross section (Fig. 4c) shows that the steps contain terraces that occur approximately half way between the billietite surface and the surface of the steps. Furthermore, the FTIR spectrum of a billietite crystal (set 1) treated for 24 h with a 0.1 mol L^{-1} Na_2CO_3 solution did not indicate the presence of $(CO_3)^{2-}$ groups, excluding the possibility of precipitation of a carbonate-bearing phase on the basal surface.

Crystals treated with electrolyte solutions of pH 2

We examined the morphology and orientation of etch pits formed on billietite crystals of set 1 and 2. However, we will only discuss in detail the morphology of the etch pits observed on billietite crystals of set 2, where they differ in orientation and morphology from those observed on billietite crystals of set 1. Hillocks as a result of a precipitation of unknown phases have been observed on all basal surfaces and their number, height and lateral dimensions vary with the type of cation in solution and the duration of the experiment. However, in this paper, we will focus on the orientation and morphology of etch pits and the relief of the basal surface after the dissolution experiment rather than on the formation of secondary phases on the surface of bllietite. In this way, we only tried to identify the phase formed in a $Pb(NO_3)_2$ solution on a billietite crystal of set 1 (see below), because the corresponding basal surface contains the highest number of hillocks of all basal surfaces treated for 1.5 h with an electrolyte solution of pH 2 (set 1).

The basal surface treated with an aqueous 0.50 mol L^{-1} $CaCl_2$ solution of pH 2

Figure 5a shows typical etch-pits on the basal (001) surface of billietite (set 1) after treatment with a 0.50 mol L^{-1} aqueous $CaCl_2$ solution of pH 2. The etch pits are elongate parallel to [010] and are in some cases bound by the edges [010], [110] and [100]. The outlines of the etch pits are generally irregular and do not display mirror symmetry. Colors indicating different depths show that the pits have steep sides and a flat bottom. The pits are connected *via* flat dissolution-channels with an average depth of ~35 nm. Etch pits formed on a billietite crystal of set 2 have identical orientations and similar morphologies, but are deeper and have larger lateral dimensions.

Figure 6 shows optical microscopy images of billietite crystals (set 2) before and after a dissolution experiment for 2 h. It is apparent that the basal surface has a high relief with deep etch-pits and grooves.

The basal surface treated with an aqueous 1.00 mol L^{-1} KCl solution of pH 2

Figure 5b shows etch features observed on the basal surface of a twinned crystal of billietite (set 1) after dissolution with an aqueous 1.00 mol L^{-1} KCl solution of pH 2 .The needle-like etch features are elongate parallel to [310] and are in some cases terminated by [110] edges. The distance between adjacent etch-pits is very small, and a cross section over an array of pits indicate deep pits with steep sides (Fig. 5b). An optical microscopy image of the billietite crystal indicates that the density of etch pits varies strongly on the basal surface. Areas with a high and low relief represent high and low densities of etch pits, respectively (Fig. 2b).

Figure 5c shows etch pits observed on the basal surface of a billietite crystal of set 2. The etch pits are elongate parallel to [100] and are defined by [100] and [310] edges. Figure 6 shows that the outline of the basal surface is nearly identical before and after the dissolution experiment for 2 h. Furthermore, the basal surface contains a low relief with no grooves and small and shallow etch-pits.

The basal surface treated with an aqueous 0.50 mol L^{-1} $MgCl_2$ solution of pH 2

Etch pits formed on billietite (set 1) in an aqueous $MgCl_2$ solution of pH 2 are elongate parallel to [100], are bound by rounded edges along their elongation, and are terminated by [010] edges (Figs. 7a, b). Colors indicating different depths of the etch pits show that the termination on [010] is in some cases irregular and is characterized by small indentations (colored dark violet). A closer inspection of Figure 7b shows that the latter dissolution-induced feature only occurs on the [010] edge, suggesting that the etch pits grow dominantly perpendicular to this direction. The outline of the etch pits generally display a mirror symmetry perpendicular to [010].

Etch pits formed on a billietite crystal of set 2 have identical orientations and similar morphologies (without indentations), but the etch pits are deeper and have larger lateral dimensions. The optical microscope images of the billietite crystal show that the edges along its basal face became more rounded during the dissolution experiment and that the treated basal surface has a high relief with a high density of deep etch-pits (Fig. 6).

The basal surface treated with an aqueous 1.00 mol L^{-1} NaCl solution of pH 2

Figures 7c and 7d show etch pits after dissolution with an aqueous 1.00 mol L^{-1} NaCl solution of pH 2 (set 1). The etch pits are elongate parallel to [100] and have the largest lateral dimensions of all pits observed in the dissolution experiments of set 1. Colors indicating different depth show that the etch pits are bound in the upper part by the edges [100], [110], [010] and [210] (pink-violet to green) and in the lower part (red) by the edges [100] and [010] (Fig. 7c). Similar to the etch pits formed in an aqueous $MgCl_2$ solution, the [010]

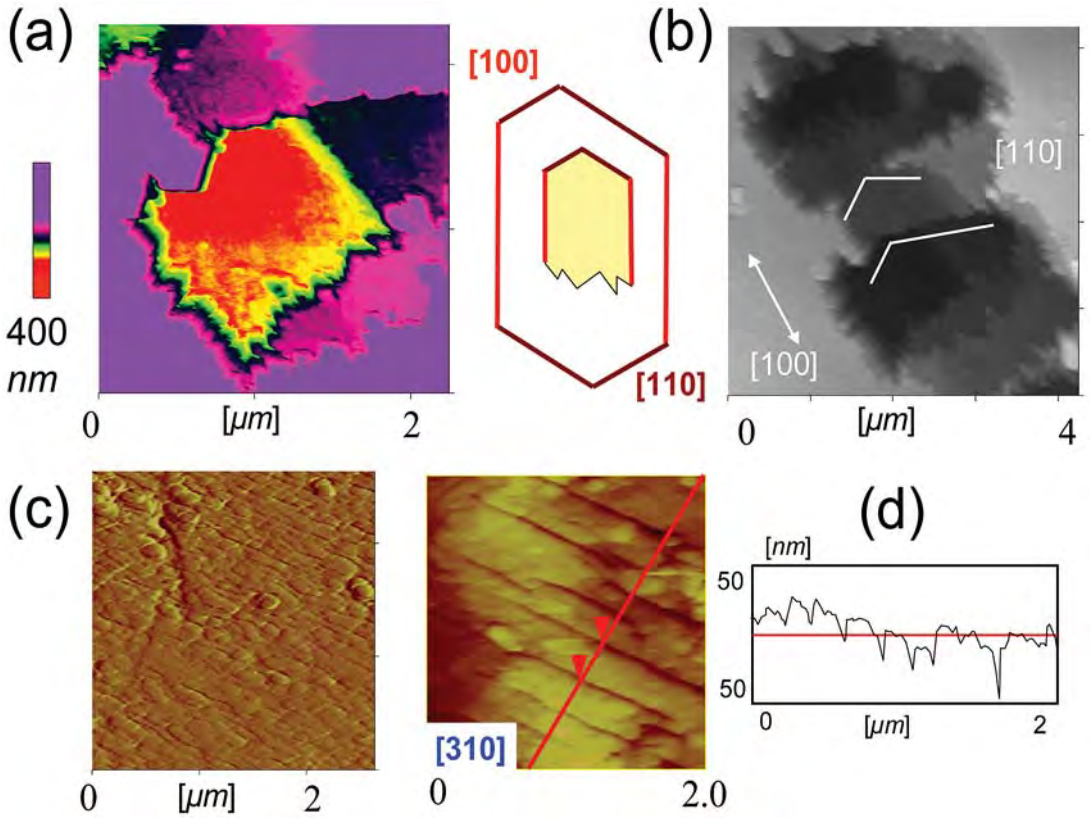

FIG. 3. (a), (b) AFM images in height mode of dissolution features on the basal surface of billietite crystals treated with aqueous solution of HCl at pH 2. The colors in (a) indicate the morphology of the pit at different depths. (c), (d) AFM images in deflection mode of (c) hillocks and (d) ripples on the basal surface of billietite crystals treated with ultrapure water. The cross section in (d) indicates the height and lateral dimensions of the ripples.

edge commonly seems irregular and is characterized by small indentations.

Etch pits formed on billietite crystals of set 2 have again identical orientation and similar morphologies but are deeper and have larger lateral dimensions. Figure 6 shows the billietite crystal before and after the dissolution experiment for 2 h. The surface of the basal face became very rough during the dissolution experiment and is characterized by deep etch-pits and grooves.

The basal surface treated with an aqueous 0.50 mol L^{-1} $Pb(NO_3)_2$ solution of pH 2

Figure 8a shows a precipitate on the surface of billietite after the dissolution experiment with an aqueous 0.50 mol L^{-1} $Pb(NO_3)_2$ solution after 1½ h (set 1). The precipitation contains small particles with a height of ~13–14 nm (not shown). A chemical analysis by LA–ICP–MS indicated a lower $^{206}Pb/^{207}Pb$ ratio in the upper surface-layers than in the deeper part of the crystal. Assuming a constant $^{206}Pb/^{207}Pb$ ratio during growth of the billietite crystal, the higher concentration of ^{207}Pb indicates $^{206}Pb/^{207}Pb$ fractionation during precipitation of the Pb-bearing phase. No etch pits were found on the basal surface of the non-freshly cleaved crystal of billietite (set 1).

Etch pits formed on the basal surface of a freshly cleaved crystal of billietite treated for 2 h with an aqueous 0.50 mol L^{-1} $Pb(NO_3)_2$ solution. The etch pits are elongate parallel to [010] and are defined by rounded edges. Figure 6 shows that after the dissolution experiment, the basal surface is slightly rougher than the basal surface after the KCl experiment. Similar to the latter experiment, the outline of the basal surface is nearly identical before and after the dissolution experiment.

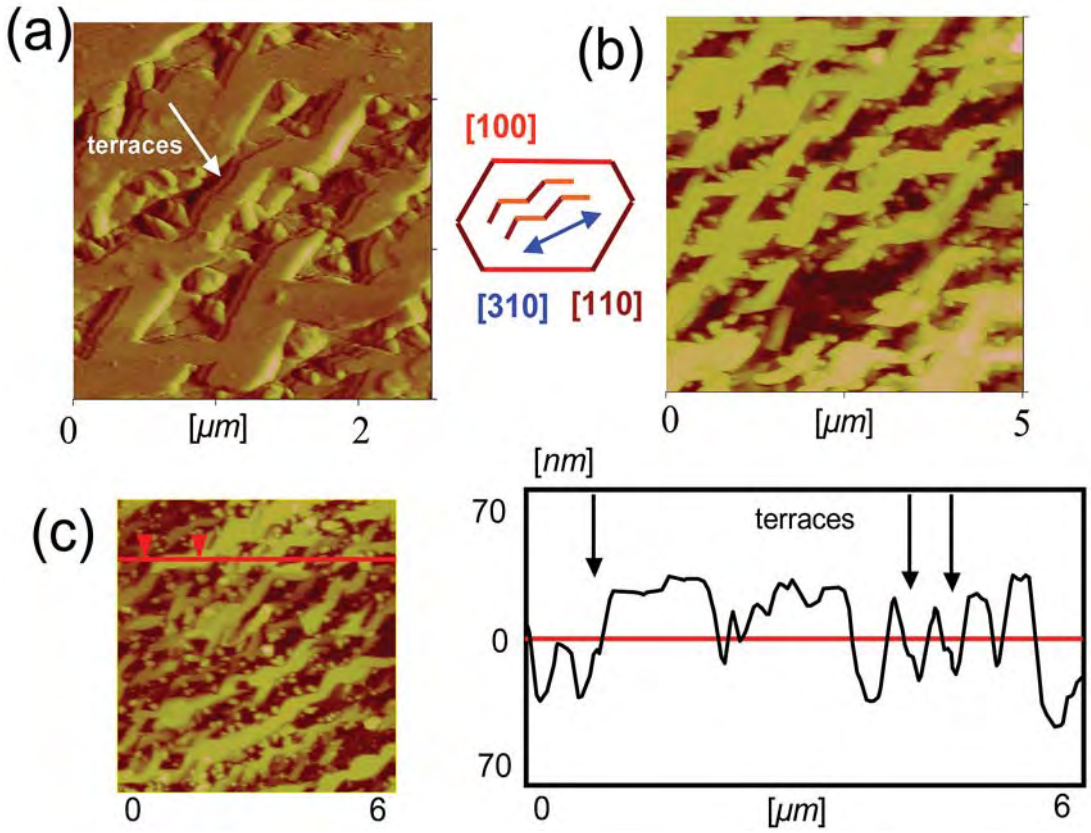

FIG. 4. AFM images of the striped pattern formed in a Na_2CO_3 solution at pH 10.5 in (a) deflection and (b) height mode; (c) cross-section of the steps, indicating the occurrence of terraces between the surface of the billietite and the steps.

The basal surface treated with an aqueous 0.50 mol L^{-1} $SrCl_2$ solution of pH 2

Figure 8c shows etch pits observed after dissolution in an aqueous 0.50 mol L^{-1} $SrCl_2$ solution of pH 2 of billietite crystals of set 1. They are elongate parallel to [010], and their terminations on the [010] edge are very irregular and are again characterized by small indentations. In cross-section, the sides of the etch pit are approximately symmetrical and merge into a flat bottom.

Figure 8d shows etch pits formed on a billietite crystal of set 2. They also are elongate parallel to [010], but their edges are more regular and parallel to [010] and [110]. Figure 6 shows that the basal face of the billietite crystal contains many small etch-pits and that their outlines are similar before and after the dissolution experiment for 2 h.

DISCUSSION

Minerals with sheets of polymerized polyhedra, such as micas, clays and uranyl-oxide-hydroxy-hydrate minerals, show different degrees of involvement of edges and the basal surface in the overall process of dissolution. Zysset & Schindler (1996), Rufe & Hochella (1999) and Bosbach *et al.* (2000) showed that dissolution of many clays and micas begins at the edges of the crystal and only occurs on the basal faces in the final stages of dissolution. Schindler *et al.* (2006b), Huertas *et al.* (1999) and Aldushin *et al.* (2004) showed that the basal surfaces of becquerelite, kaolinite and "apophylite", respectively, are involved significantly in the overall dissolution process. Similar to becquerelite, the involvement of edges and the basal surface of billietite crystals varies with pH and the type of cation in solution (Fig. 6). Dissolution on edges along

the basal surface of billietite crystals occurs mainly in aqueous $MgCl_2$ and $CaCl_2$ solutions of pH 2, whereas dissolution occurs dominantly on the basal surfaces of crystals treated with NaCl, KCl, $Pb(NO_3)_2$ and $SrCl_2$ solutions of pH 2.

Change in dissolution features on the basal surface with pH

The dissolution experiments on the basal surface of curite and becquerelite show that formation of hillocks is independent of the type of anion and cation in solution and of the ionic strength of the solution. Furthermore, the formation of etch pits (rather than hillocks) is favored by increased protonation of edges and the basal surface (Schindler *et al.* 2004a, b). The latter observation can be also recognized on the basal surface of billietite: etch pits form in a HCl solution of pH 2, whereas hillocks, ripples and steps form in aqueous H_2O and Na_2CO_3 solutions. Recent XPS measurements (M. Schindler, unpubl. data) showed that the hillocks formed in ultrapure water are the product of a schoepite-type phase $(UO_3)•2H_2O$ and that the ripples are the product of a Na-bearing uranyl-hydroxy-hydrate phase. The latter observation agrees with the results of the FTIR spectra, which did not indicate the presence of $(CO_3)^{2-}$ groups on surfaces treated with a solution of Na_2CO_3.

Etch pits formed on freshly and non-freshly cleaved crystals of billietite

We showed above that freshly and non-freshly cleaved crystals of billietite treated with the same solution do not necessarily contain etch pits of identical morphology. The most apparent differences in the

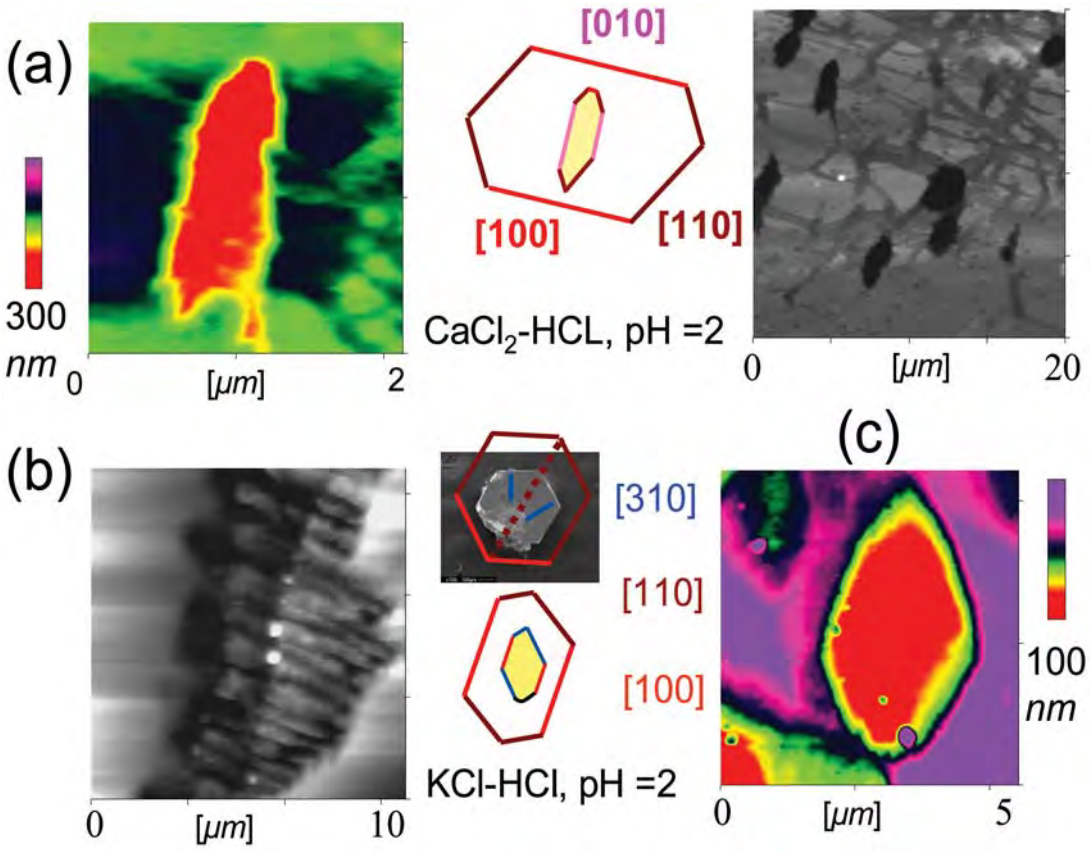

FIG. 5. (a) AFM images in height mode of etch pits formed in aqueous solution $CaCl_2$ at pH 2.0 and their orientation on the basal surface of billietite. On the left, the colors indicate the morphology of the pit at different depth. (b), (c) AFM images in height mode of etch pits formed in aqueous solution of KCl at pH 2.0 on a non-freshly cleaved surface (b) and a freshly cleaved surface (c). The colors indicate the morphology of the pit at different depth and their orientation on the basal surface of billietite.

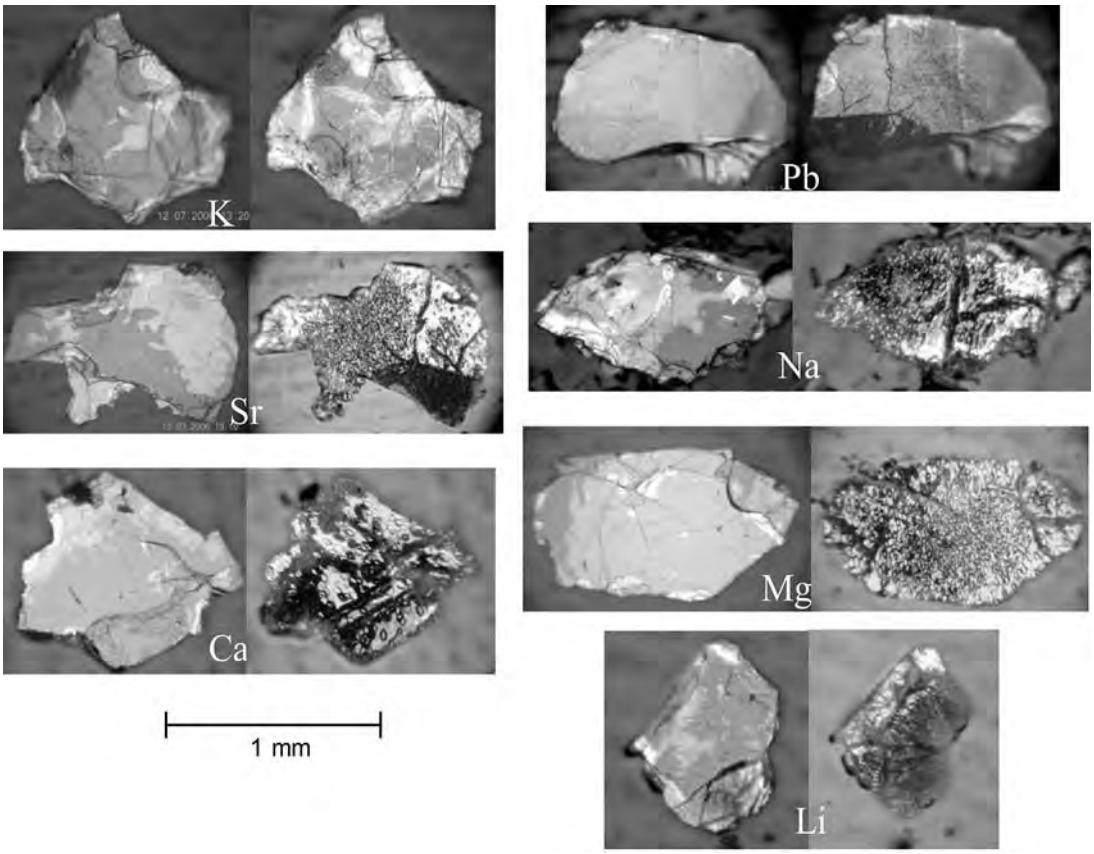

FIG. 6. Optical-reflection microscopy images of billietite crystals before (left-hand side) and after (right-hand side) dissolution experiments in electrolyte solutions of pH 2 for 2 h; the major cation in the electrolyte solution is indicated in the optical image.

morphology of etch pits are those formed in aqueous KCl and $SrCl_2$ solutions of pH 2. In both cases, the morphology of the etch pits formed on the basal surfaces of the non-freshly cleaved crystals were more irregular than on the surfaces of the freshly cleaved crystals. The growth of an etch pit and the stability of the edges defining the etch pits thus can significantly differ between altered (non-freshly cleaved) and non-altered (freshly cleaved) surfaces. Furthermore, we did not observe the formation of etch pits on a non-freshly cleaved surface treated with an aqueous 0.50 mol L^{-1} solution of $Pb(NO_3)_2$ for 1.5 h, which may also indicate that the nucleation of an etch pit is affected by the degree of alteration of the surface of billietite. However, the orientation of the etch pits formed on surfaces treated with the same electrolyte solutions were identical, with the exception of the surface treated with an aqueous KCl solution. This observation shows that the effect of cations on the growth of the etch pits (see below) is independent of the degree of alteration of the surface of billietite.

Orientation of etch pits on becquerelite and billietite

The orientation of etch pits on the basal surfaces of becquerelite and billietite treated with different electrolyte solutions can be summarized as follows: Etch pits elongate parallel to [100] form in aqueous solutions of KCl, NaCl, and $MgCl_2$, and etch pits elongate parallel to [010] form in aqueous solutions of $SrCl_2$, $Pb(NO_3)_2$ and $CaCl_2$. Note that etch pits on the basal surface of becquerelite were formed in a Ca-containing solution during synthesis. However, etch features on a crystal of billietite of set 1 formed in an aqueous KCl solution of pH 2 differ: they are elongate parallel to [310], whereas they are elongate parallel to [100] on the surfaces of becquerelite and a billietite crystal of set 2. However, the [310] edge is one of the dominant edges that defines

the morphology of etch pits on the basal surface of the billietite crystals of set 2 and of the becquerelite treated with an aqueous KCl solution. Its occurrence on the basal face of becquerelite and billietite suggests a high stability of the edge in the presence of K^+ cations on the basal surface of both minerals.

Schindler *et al.* (2006b) noted that on the basal surface of becquerelite, all monovalent cations in solution resulted in etch pits parallel to [100] (Na, K), divalent cations most different in ionic radius to $^{[8]}$Ca resulted in etch pits parallel to [100] (Ba, Mg), and cations most similar in ionic radius to $^{[8]}$Ca produced etch pits parallel to [010] (Ca, Sr and Pb^{2+}). Etch pits on the basal surface of billietite show the same orientation in the presence of the corresponding cation, with the exception of the etch pits formed on a non-freshly cleaved surface treated with an aqueous KCl solution.

Figure 9 summarizes the observations on the orientation of etch pits formed in $BaCl_2$ and $CaCl_2$ solutions and on the elongation of billietite and becquerelite crystals:

(a) billietite crystals grown in a Ba-bearing solution and etch pits formed on the basal surface of becquerelite in a $BaCl_2$ solution are parallel to the rows of Ba atoms in the bulk structures of billietite and becquerelite;

(b) becquerelite crystals grown in a Ca solution and etch pits formed on the basal surface of billietite in a $CaCl_2$ solution are parallel to the rows of Ca atoms in the bulk structures of becquerelite and billietite.

Adsorption model

Schindler *et al.* (2006b) developed a model for the adsorption of cations in solution at specific surface-sites on the basal surface of becquerelite. Using a protonation

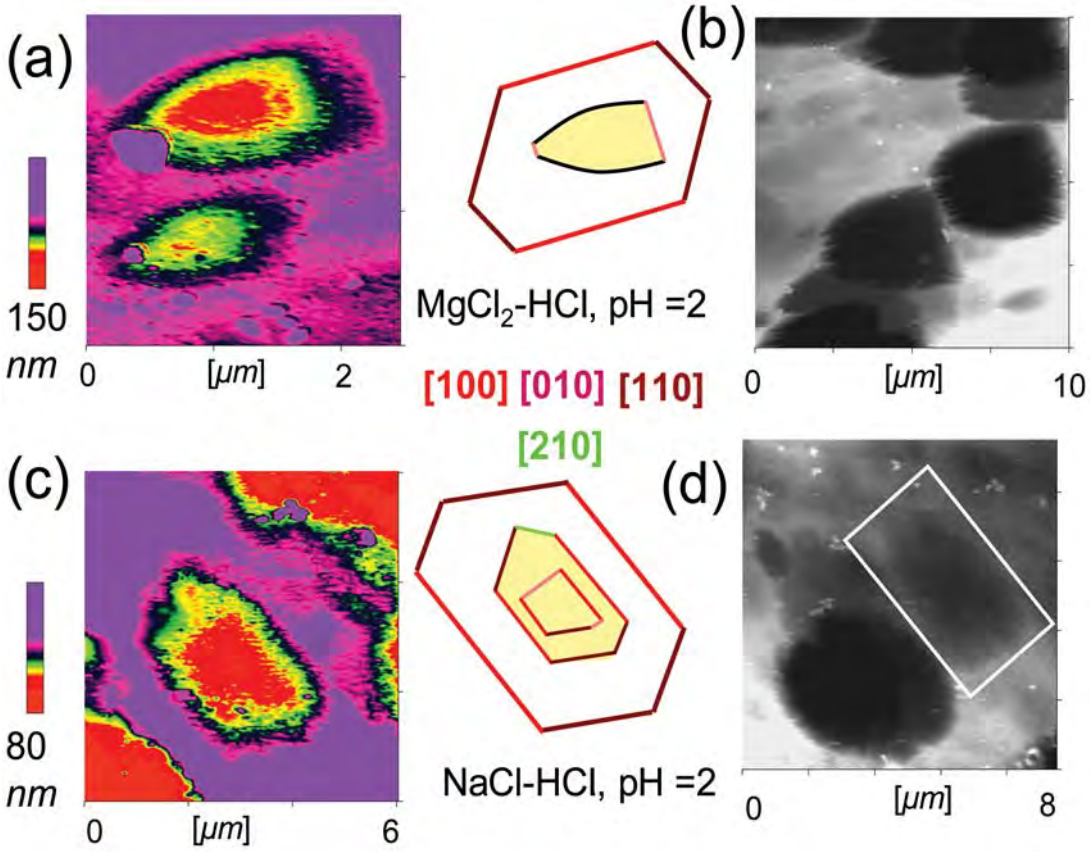

FIG. 7. (a) AFM images in height mode of etch pits formed in aqueous solution of $MgCl_2$ at pH 2.0 and their orientation on the basal surface of becquerelite. On the left, the colors indicate the morphology of the pit at different depth. (b) AFM images of etch pits formed in aqueous solution of NaCl of pH 2.0 and their orientation on the basal surface of becquerelite. The type of images on the left and right is the same as in 7(a). The locations of the etch pits in (c) are indicated with a white frame (d).

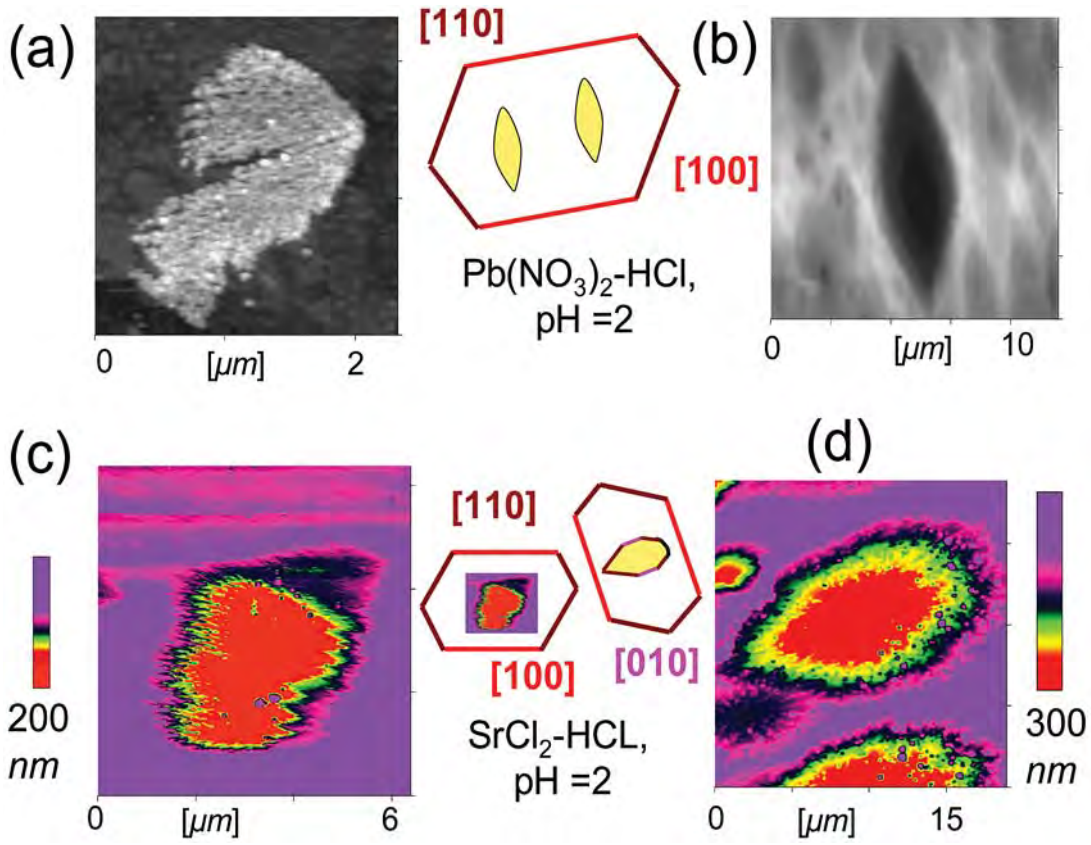

FIG. 8. AFM images in height mode from the basal surfaces treated with an aqueous solution of $Pb(NO_3)_2$ at pH 2.0. (a) Pb-bearing precipitate formed on a non-freshly cleaved surface. (b) Etch pits formed on a freshly cleaved surface. (c), (d) AFM images in height mode of etch pits formed in aqueous solution of $SrCl_2$ at pH 2.0 and their orientation on the basal surface of billietite, (c) on a non-freshly cleaved surface, and (d) on a freshly cleaved surface. The colors indicate the morphology of the pit at various depths.

model for the oxygen atoms on the basal surface and along its edges, they argued that adsorbed cations most likely bond to the oxygen atoms of the uranyl groups. They further noted that in the bulk structures of minerals of the becquerelite group, the interstitial cations bond only to oxygen atoms of the uranyl group or to (H_2O) groups in the interlayer. As an example, they showed that Ca and Ba occur at the designated sites *A* and *B* in the interlayer of becquerelite and billietite (Figs. 9b, e). These sites are related to the distance between the apical O-atoms; hence, the larger Ba atom occurs only at the *A* site, which results in rows of Ba parallel to [100], whereas the smaller Ca atom occurs at the *A* and *B* sites, which results in rows of Ca parallel to [010] (Figs. 9b, e). Schindler *et al.* (2006b) showed that if adsorbed Ba and Ca adopt the same arrangement on the surface as they do in the bulk structure, they would also bond to different groups of polyhedra (the red and yellow clusters in Figs. 9c, f). Hence, adsorption of cations at these surface sites would not only prevent the formation of activated sites (through protonation) parallel to the row of cations, it would also prevent the detachment of groups of polyhedra perpendicular to the rows of cations. Using this adsorption model and the observed orientation of etch pits, Schindler *et al.* (2006b) predicted that during the dissolution process, Mg, Na and K are arranged in rows parallel to [100], whereas Sr and Pb^{2+} are arranged in rows parallel to [010].

Morphology of etch pits on becquerelite and billietite

Schindler *et al.* (2006b) showed that etch pits formed on the basal face of becquerelite in aqueous $BaCl_2$, KCl, $SrCl_2$ and $MgCl_2$ solutions are bound by regular edges, and the outline of the etch pits generally displays a

mirror symmetry. The morphology of etch pits observed on the basal surfaces of billietite crystals of set 2 are similar. For example, etch pits formed in a KCl solution are highly elongate, etch pits formed in an aqueous NaCl solution have a large rectangular outline, etch pits formed in $SrCl_2$ solutions have large lateral dimensions, etch pits formed in $Pb(NO_3)_2$ solutions are rounded, and etch pits formed in an aqueous $MgCl_2$ solution are small and have a cigar- to rectangular-shaped outline.

Surface structure and role of the interstitial cations

We are now able to answer the question whether becquerelite and billietite have the same surface-structure and what is the effect of the interstitial cations on the orientation and morphology of dissolution features. Similar orientations and morphologies of etch pits on the basal surfaces of billietite and becquerelite indicate that (1) the same type of cation in solution is adsorbed at similar surface-sites; (2) surface sites are arranged in a similar fashion and are independent of the type of interstitial cation; (3) the arrangement of the interstitial cations in the bulk structure of both minerals has no effect on the orientation of etch pits.

The occurrence of more rounded and irregular edges along etch pits on billietite crystals of set 1 indicates that altered (non-freshly cleaved) surfaces of billietite crystals have a different surface-structure than unaltered (freshly cleaved) crystals of billietite and becquerelite (see above).

Dimensions of etch pits on the basal face of billietite

Schindler *et al.* (2006a, b) showed that the average area and the depth of etch pits can be used to define the degree of dissolution of edges and the change in relief of a basal surface. Here, higher relief of an etch pit is not the result of a higher rate of dissolution perpendicular to the sheets; rather, it is an expression of the difference between the lowering of the surrounding surface and the growth of the etch pit perpendicular to the sheet. Figure 10 shows the area *versus* depth for etch pits formed on billietite crystals. Etch pits formed in aqueous NaCl, and $SrCl_2$ solutions have the largest ratio between area and depth, which indicates a small difference between the lowering of the surrounding surface and growth of the etch pits perpendicular to the sheet. Etch pits formed in aqueous $CaCl_2$ and KCl solutions have the smallest ratio between area and depth, which indicates a large difference between the lowering of the surrounding surface and the growth of etch pits perpendicular to the sheet. The ratios between area and depth of etch pits formed in NaCl, $SrCl_2$ and KCl solutions are similar to the dimensional ratios of etch pits formed on the basal surface of becquerelite. A major difference occurs in the dimensional ratios of etch pits formed in $MgCl_2$ solution: the etch pits on the surface of billietite have a much larger area : depth ratio than etch pits on the becquerelite surface.

Factors controlling the dissolution rate of a single crystal

Schindler *et al.* (2006b) discussed the factors that control the dissolution rate of single crystals: crystal size, roughness, ionic strength and nature of the cation in solution. The surfaces of the billietite crystals used in the dissolution experiments for 2 h had similar dimensions and roughness before the dissolution experiment, and the ratios between the volume of solution (10 mL) and the dimensions of the single crystals were extremely high. Thus, the relief of dissolution features on the basal surfaces should be mainly a product of the type of cation in solution (rather than a product of the dimensions and roughness of the surface).

The effect of different cations in solution on the relief of dissolution features

Schindler *et al.* (2006b) distinguished between dissolution features on the basal surface and dissolution features on the edges along the basal surface of becquerelite. Closer inspection of the optical images (Fig. 6) shows that dissolution features on edge and basal surfaces of billietite crystals cannot easily be differentiated. Hence, we will examine the relief of dissolution features on the basal surfaces of the billietite crystals without distinguishing between features on edges and basal surfaces.

Using the general appearance of the basal surface, we arranged the images of the crystals so that the degree of dissolution on the basal surface and edges increases from left to right and from top to bottom. It is apparent that the relief of dissolution features on the basal surface and edges formed in aqueous solutions of simple salts increases in the sequence KCl < $Pb(NO_3)_2$ < $SrCl_2$ < NaCl < $CaCl_2$ = $MgCl_2$, suggesting that the relief of the basal surface inversely correlates with the size of the cation in solution (Table 2). In order to test if this observation is generally true for other cations, we also carried out a dissolution experiment in a LiCl solution ($^{[6]}$Li = 0.76 Å) of pH 2 for 2 h. Figure 6 shows the crystals before and after the dissolution experiment. It is apparent that the overall relief of the basal surface and its edges is higher than the relief of the surface treated with a NaCl solution and similar to the relief of the surfaces treated with $CaCl_2$ and $MgCl_2$ solution. In this way, the relief of the crystals increases in the sequence KCl < $Pb(NO_3)_2$ < $SrCl_2$ < NaCl < $CaCl_2$ = $MgCl_2$= LiCl, in accord with the observation that the relief inversely correlates with the size of the cations in solution.

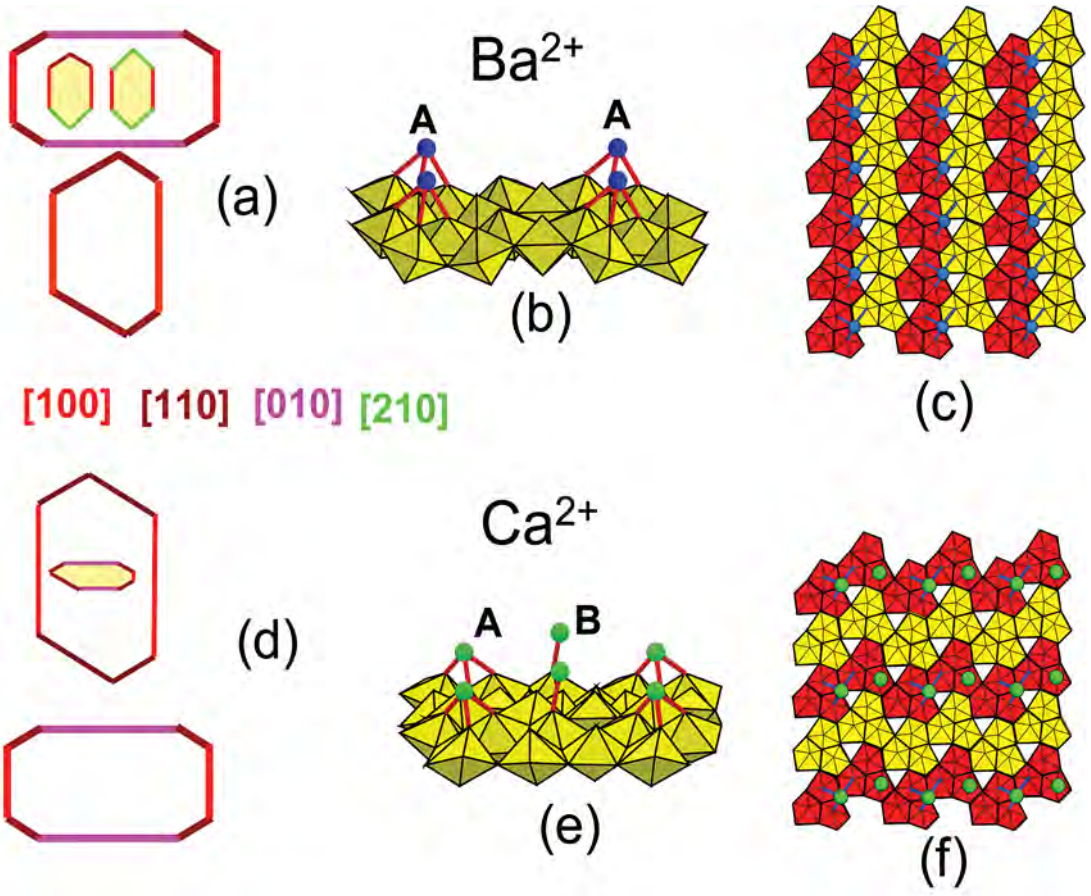

FIG. 9. (a) – (c). From left to right, morphologies of a billietite crystal (bottom) and of etch pits formed on the basal surface of becquerelite in the presence of Ba^{2+} (top) (a); Ba^{2+} at position A on the surface of the uranyl sheet in the bulk structure of billietite (b). The Ba^{2+} atoms are shown as blue circles, and the bonds between Ba^{2+} and O atoms of the uranyl groups are shown as red lines. There are rows of Ba^{2+} atoms parallel to [100] in the bulk structure of billietite (c). (d) – (f) From left to right, morphology of becquerelite crystals (bottom) and of an etch pit formed on the basal surface of billietite in the presence of Ca^{2+} (top) (d). There are Ca^{2+} atoms at positions A and B on the surface of the uranyl sheet in the bulk structure of becquerelite (e). The Ca^{2+} atoms are shown as green circles, and the bonds between Ca^{2+} and O atoms of the uranyl groups are shown as red lines. Rows of Ca^{2+} atoms are parallel to [010] in the bulk structure of becquerelite (f). Clusters of three polymerized uranyl-bearing polyhedra are indicated in yellow and red in the images of the sheets of polymerized uranyl polyhedra on the right.

A comparison between the dissolution features of the uranyl minerals billietite, becquerelite, uranophane-α, fourmarierite and synthetic $Pb_2(H_2O)[(UO_2)_{10}UO_{12}(OH)_6(H_2O)_2]$ and a detailed crystal-chemical model for the inverse correlation between relief and the size of the cations in solution are given in Schindler *et al.* (2007).

CONCLUSIONS

The dissolution experiments on single crystals of billietite at different pH and with different cations in solution show the following features on the basal surface and its edges:

(1) Hillocks and ripples form on the basal surface in ultrapure water.

(2) A striped pattern of steps form on the basal surface in a Na_2CO_3 solution.

(3) Etch pits form only in solutions of pH 2, indicating that their formation is favored by an increase in the activity of protons in solution.

(4) Etch pits that form on the altered surfaces of non-freshly cleaved crystals of billietite rarely display symmetry elements of the bulk structure, which indicates that the stability of edges and the growth of an etch pit are affected by the degree of alteration of a surface.

(5) Etch pits that form in aqueous NaCl, KCl and $MgCl_2$ solutions are elongate parallel to [100], suggesting that adsorbed cations are arranged in rows parallel to [100] on the basal surface of billietite.

(6) Etch pits that form in aqueous $CaCl_2$, $Pb(NO_3)_2$ and $SrCl_2$ solutions are elongate parallel to [010], suggesting that adsorbed cations are arranged in rows parallel to [010] on the basal surface of billietite.

(7) Hillocks occur as a result of precipitation processes on all basal surfaces examined, whereas an unknown Pb-bearing phase precipitates on the basal surface in an aqueous solution of $Pb(NO_3)_2$.

(8) The relief of the dissolution features on edges of the basal surface increases in the sequence KCl < $Pb(NO_3)_2$ < $SrCl_2$ < NaCl < $CaCl_2$ = $MgCl_2$ = LiCl.

TABLE 2. IONIC RADII (Å) AND CHARACTERISTIC COORDINATION OF CATIONS IN URANYL OXIDE MINERALS

Cations	Ionic radius*
$^{[7]}K^+$, $^{[8]}K^+$	1.46, 1.51
$^{[8]}Pb^{2+}$, $^{[10]}Pb^{2+}$	1.29, 1.40
$^{[8]}Sr^{2+}$, $^{[10]}Sr^{2+}$	1.26, 1.36
$^{[6]}Ca^{2+}$	1.00
$^{[6]}Na^+$	1.02
$^{[6]}Li^+$	0.76
$^{[6]}Mg^{2+}$	0.72

* Shannon (1976), Schindler & Hawthorne (2004).

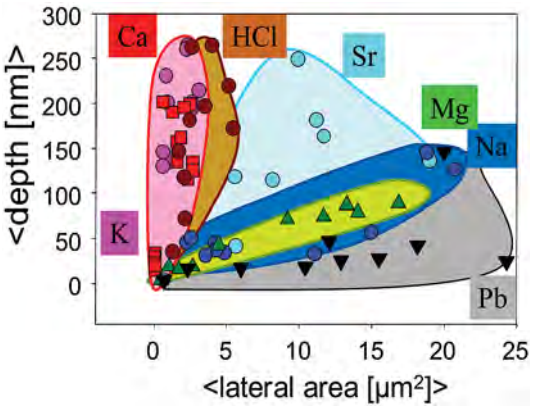

FIG. 10. Average area as a function of average depth for etch pits formed in electrolyte solution of pH 2; the major cations in solution are shown beside the colored areas.

ACKNOWLEDGEMENTS

We thank the Canadian Museum of Nature for the crystals used in our project. This work was supported by a Canada Research Chair in Crystallography and Mineralogy and by a Discovery Grant to FCH from the Natural Sciences and Engineering Research Council of Canada, and by a Canada Foundation for Innovation Grant to FCH. We thank David Kreller for assistance on the AFM, Sergio R. Mejia for help on the SEM, and Sasha Herwig and Neil A. Ball for assistance with the IR spectrometer. We also thank Editor Bob Martin and an unknown reviewer for their comments on the manuscript.

REFERENCES

ALDUSHIN, K., JORDAN, G., RAMENSEE, W., SCHMAHL, W.W. & BECKER, H.-W. (2004): Apophyllite (001) surface alteration in aqueous solutions studied by HAFM. *Geochim. Cosmochim. Acta* **68**, 217-226.

BOSBACH, D., CHARLET, L., BICKMORE, B. & HOCHELLA, M.F., JR. (2000): The dissolution of hectorite: in-situ, real time observations using atomic force microscopy. *Chem. Geol.* **151**, 143-160.

BUCK, E.C., FINCH, R.J., FINN, P.A. & BATES, J.K. (1998): Retention of neptunium in uranyl alteration phases formed during spent fuel corrosion. *In* Scientific Basis for Nuclear Waste Management XXI. (I.G. McKinley & C.H. McCombie, eds.). *Mater. Res. Soc., Symp. Proc.* **506**, 83-91.

BURNS, P.C. (1998): The structure of compreignacite $K_2[(UO_2)_3O_2(OH)_3]_2(H_2O)_7$. *Can. Mineral.* **36**, 1061-1067.

BURNS, P.C. (1999): The crystal chemistry of uranium. *In* Uranium: Mineralogy, Geochemistry and the Environment (P.C. Burns & R. Finch, eds.). *Rev. Mineral.* **38**, 23-90.

BURNS, P.C., DEELY, K.M. & SKANTHAKUMAR, S. (2004): Neptunium incorporation into uranyl compounds that form as alteration products of spent nuclear fuel: implications for geologic repository performance. *Radiochim. Acta* **92**, 151-159.

BURNS, P.C., EWING, R.C. & MILLER, M.L. (1997): Incorporation mechanims of actinide elements into the structures of U^{6+} phases formed during the oxidation of spent nuclear fuel. *J. Nucl. Mater.* **245**, 1-9.

BURNS, P.C. & LI, YAPING (2002): The structures of becquerelite and Sr-exchanged becquerelite. *Am. Mineral.* **87**, 550-557.

CASAS, I., BRUNO, J., CERA, E., FINCH, R.J. & EWING, R.C. (1997): Characterization and dissolution behavior of a becquerelite from Shinkolobwe, Zaire. *Geochim. Cosmochim. Acta* **61**, 3879-3884.

CHEN, F., BURNS, P.C. & EWING, R.C. (1999): ^{79}Se: geochemical and crystallo-chemical retardation mechanisms. *J. Nucl. Mater.* **275**, 81-94.

CHEN, F., BURNS, P.C. & EWING, R.C. (2000): Near-field behavior of ^{99}Tc during the oxidative alteration of spent nuclear fuel. *J. Nucl. Mater.* **278**, 225-232.

DOUGLAS, M., CLARK, S.B., FRIESE, J.I., AREY, B.W., BUCK, E.C., HANSON, B.D., UTSUNOMIYA, S. & EWING R.C. (2005) Microscale characterization of uranium(VI) silicate solids and associated neptunium(V). *Radiochim. Acta* **93**, 265-272.

FINCH, R.J., BUCK, E.C., FINN, P.A. & BATES, J.K. (1999): Oxidative corrosion of spent UO_2 fuel in vapor and dripping groundwater at 90°C. *In* Scientific Basis for Nuclear Waste Management XXII (D.J. Wronkiewicz & J.H. Lee, eds.). *Mater. Res. Soc., Symp. Proc.* **556**, 431-439.

FINCH, R.J., BURNS, P.C., HAWTHORNE, F.C. & EWING, R.C. (2006): Refinement of the crystal structure of billietite, $Ba[(UO_2)_6O_4(OH)_6](H_2O)_8$. *Can. Mineral.* **44**, 1197-1206.

FINCH, R.J. & EWING, R.C. (1992): The corrosion of uraninite under oxidizing conditions. *J. Nucl. Mater.* **190**, 133-156.

FINN, P.A., HOH, J.C., WOLF, S.F., SLATER, S.A. & BATES, J.K. (1996): The release of uranium, plutonium, cesium, strontium, technetium and iodine from spent fuel under unsaturated conditions. *Radiochim. Acta* **74**, 65-71.

FRONDEL, C. (1958): Systematic mineralogy of uranium and thorium. *U.S Geol. Surv., Bull.* **1064**.

GIAMMAR, D.E. & HERING, J.G. (2004): Influence of dissolved sodium and cesium on uranyl oxide hydrate solubility. *Environ. Sci. Technol.* **38**, 171-179.

GUSTAFSSON, J.P. (2003): Visual MINTEQ, Version 2.22. KTH, Department of Land and Water Resources Engineering, Stockholm, Sweden. http://www.trinityminerals.com /sm2001/uranium.shtml

HUERTAS, F.J., CHOU, L. & WOLLAST, R. (1999): Mechanism of kaolinite dissolution at room temperature and pressure. II. Kinetic study. *Geochim. Cosmochim. Acta* **63**, 3261-3271.

PAGOAGA, M.K., APPLEMAN, D.E. & STEWART, J.M. (1987): Crystal structure and crystal chemistry of the uranyl oxide hydrates becquerelite, billietite and protasite. *Am. Mineral.* **72**, 1230-1238.

PARKHURST, D.L. (2003): PHREEQC – a computer program for speciation, reaction path, advective transport and inverse geochemical calculations. *U.S. Geol. Surv*. [http://wwwbrr.cr.usgs.gov/projects/GWC coupled/phreeqc/index.html].

PERLOFF, L. (1998): *The Photo-Atlas of Minerals* (A.R. Kampf & G. Gerhold, eds.). The Gem and Mineral Council, Los Angeles County Museum of Natural History, Los Angeles, California.

PROTAS, J. (1964): Une nouvelle espèce minérale: la compreignacite, $K_2O{\bullet}6UO_3{\bullet}11H_2O$. *Bull. Minéral.* **87**, 365-371.

ROH, Y., LEE, S.R., CHOI, S.K., ELLES, M.P. & LEE, S.Y. (2000): Physicochemical and mineralogical characterization of uranium-contaminated soils. *Soil Sed. Contam.* **9**, 463-486.

RUFE, E. & HOCHELLA, M., JR. (1999): Quantitative assessment of reactive surface area of phlogopite dissolution during acid dissolution. *Science* **285**, 874-876.

SANDINO, M.C.A. & BRUNO, J. (1992): The solubility of $(UO_2)_3(PO_4)_2{\bullet}4H_2O(s)$ and the formation of U(VI) phosphate complexes: their influence in uranium speciation in natural waters. *Geochim. Cosmochim. Acta* **56**, 4135-4145.

SANDINO, M.C.A. & GRAMBOW, B. (1994): Solubility equilibria in the U(VI)–Ca–K–Cl–H_2O system: transformation of schoepite into becquerelite and compreignacite. *Radiochim.* **66/67**, 37-43.

SCHINDLER, M. & HAWTHORNE, F.C. (2004): A bond-valence approach to uranyl-oxide hydroxy-hydrate minerals: chemical composition and occurrence. *Can. Mineral.* **42**, 1601-1627.

SCHINDLER, M., HAWTHORNE, F.C., BURNS, P.C. & MAURICE, P.A. (2006b): Dissolution of uranyl-hydroxy-hydrate minerals. II. Becquerelite. *Can. Mineral.* **44**, 1207-1225.

SCHINDLER, M., HAWTHORNE, F.C., BURNS, P.C. & MAURICE, P.A. (2007): Dissolution of uranyl-hydroxy-hydrate minerals. IV. Fourmarierite and synthetic $Pb_2(H_2O)[(UO_2)_{10}UO_{12}(OH)_6(H_2O)_2]$. *Can. Mineral.* **45**, 963-981.

SCHINDLER, M., HAWTHORNE, F.C., PUTNIS, C. & PUTNIS, A. (2004c): Growth of uranyl-hydroxy-hydrate and uranyl-carbonate minerals on the (104) calcite surface. *Can. Mineral.* **42**, 1683-1697.

SCHINDLER, M., MANDALIEV, P., HAWTHORNE, F.C. & PUTNIS, A. (2006a): Dissolution of uranyl-hydroxy-hydrate minerals. I. Curite. *Can. Mineral.* **44**, 415-431.

SCHINDLER, M., MUTTER, A., HAWTHORNE, F.C. & PUTNIS, A. (2004a): Prediction of crystal morphology of complex uranyl-sheet minerals. I. Theory. *Can. Mineral.* **42**, 1629-1649.

SCHINDLER, M., MUTTER, A., HAWTHORNE, F.C. & PUTNIS, A. (2004b): Prediction of crystal morphology of complex uranyl-sheet minerals. II. Observation. *Can. Mineral.* **42**, 1651-1666.

SCHINDLER, M. & PUTNIS, A. (2004): Crystal growth of schoepite on the (104) surface of calcite. *Can. Mineral.* **42**, 1629-1649.

SCHOEP, A. & STRADIOT, S. (1948): Additional data on the properties of becquerelite and billietite. *Am. Mineral.* **33**, 503-507.

SHANNON, R.D. (1976): Revised effective ionic radii in halides and chalcogenides. *Acta Crystallogr*. **A32**, 751-767.

STUMM, W. (1992): *Chemistry of the Solid–Water Interface*. John Wiley & Sons, New York, N.Y. (p. 428).

TORRERO, M.E., CASAS, I., DE PABLO, J., SANDINO, M.C.A. & GRAMBOW, B. (1994): A comparison between unirradiated UO_2(s) and schoepite solubilities in 1 m NaCl medium. *Radiochim. Acta* **66/67**, 29-35.

VOCHTEN, R, VAN HAVERBEKE, L. & VAN SPRINGEL, K. (1991): Transformation of chernikovite into parsonsite and study of its solubility product. *Neues Jahrb. Mineral., Monatsh.*, 551-558.

VOCHTEN, R, VAN HAVERBEKE, L., VAN SPRINGEL, K., BLATON, N. & PEETERS, O.M. (1995): The structure and physicochemical characteristics of synthetic zippeite. *Can. Mineral.* **33**, 1091-1101.

WRONKIEWICZ, D.J., BATES, J.K. WOLF, S.F. & BUCK, E.C. (1996): Ten year results from unsaturated drip tests with UO_2 at 90°C: implications for the corrosion of spent nuclear fuel. *J. Nucl. Mater.* **238**, 78-95.

YAMAKAWA, I. & TRAINA, S.J. (2001): Precipitation processes of uranium in highly alkaline solutions: possible chemical reactions occurring in the Hanford vadose zone. *Am. Chem. Soc., 222nd Nat. Meeting* (*Chicago*), *GEOC–055, Abstr.*

ZYSSET, M. & SCHINDLER, P.W. (1996): The proton promoted dissolution kinetics of K-montmorillonite. *Geochim. Cosmochim. Acta* **60**, 921-931.

Received October 6, 2005, revised manuscript accepted January 30, 2007.